Mon. Not. R. Astron. Soc. **000**, 1–9 (2015) Printed 30 September 2016 (MN LATEX style file v2.2)

On the Link Between Energy Equipartition and Radial Variation in the Stellar Mass Function of Star Clusters

Jeremy J. Webb & Enrico Vesperini ⋆
Department of Astronomy, Indiana University, Swain West, 727 E. 3rd Street, IN 47405 Bloomington, USA

arXiv:1609.09082v1 [astro-ph.GA] 28 Sep 2016

30 September 2016

ABSTRACT

We make use of N-body simulations to determine the relationship between two observable parameters that are used to quantify mass segregation and energy equipartition in star clusters. Mass segregation can be quantified by measuring how the slope of a cluster's stellar mass function α changes with clustercentric distance r, and then calculating $\delta_\alpha = \frac{d\alpha(r)}{dln(r/r_m)}$ where r_m is the cluster's half-mass radius. The degree of energy equipartition in a cluster is quantified by η, which is a measure of how stellar velocity dispersion σ depends on stellar mass m via $\sigma(m) \propto m^{-\eta}$. Through a suite of N-body star cluster simulations with a range of initial sizes, binary fractions, orbits, black hole retention fractions, and initial mass functions, we present the co-evolution of δ_α and η. We find that measurements of the global η are strongly affected by the radial dependence of σ and mean stellar mass and the relationship between η and δ_α depends mainly on the cluster's initial conditions and the tidal field. Within r_m, where these effects are minimized, we find that η and δ_α initially share a linear relationship. However, once the degree of mass segregation increases such that the radial dependence of σ and mean stellar mass become a factor within r_m, or the cluster undergoes core collapse, the relationship breaks down. We propose a method for determining η within r_m from an observational measurement of δ_α. In cases where η and δ_α can be measured independently, this new method offers a way of measuring the cluster's dynamical state.

Key words: methods: statistical stars: statistics globular clusters: general

1 INTRODUCTION

Two-body gravitational interactions between stars within star clusters is one of the main dynamical processes governing their long-term evolution. Over time, two-body interactions result in the stellar population evolving towards a state of energy equipartition on a timescale commonly referred to as a cluster's relaxation time (Spitzer 1987). A natural by-product of two-body relaxation is that the cluster also becomes mass segregated. Mass segregation occurs because through two-body interactions, massive stars lose kinetic energy to less massive stars and fall inwards towards the centre of the cluster. Conversely, lower mass stars that have had their kinetic energy increased migrate outwards. Therefore the effects of two-body relaxation are expected to imprint a mass dependence in both the kinematical properties and the radial distribution of stars within a star cluster. The strength of this mass dependence evolves with the dynamical age of a cluster, and should be larger for clusters in the more advanced stages of their dynamical evolution.

In a star cluster which has reached a state of complete energy equipartition, stars at a given distance from the cluster centre will have a mass dependent velocity dispersion scaling as $\sigma(m) \propto m^{-\eta}$, with $\eta = 0.5$. Some simplified two-component systems have been shown to reach $\eta = 0.5$, however the conditions must be idealized such that the cluster does not under-go core collapse with heavier stars becoming self-gravitating (Spitzer 1969; Spitzer & Hart 1971; Lightman & Fall 1978; Inagaki & Wiyanto 1984). On the other hand, a number of studies have shown that for systems containing stars with a spectrum of masses following realistic stellar initial mass functions (IMFs) complete energy equipartition will never be reached (Vishniac 1978; Inagaki & Saslaw 1985; Watters et al. 2000; Fregeau et al. 2002; Baumgardt & Makino 2003; Khalisi et al. 2007; Parker et al. 2016; Spera et al. 2016). In a recent study based on direct N-body simulations of multi-mass star clusters, Trenti & van der Marel (2013) explored a wide range

⋆ E-mail: jerjwebb@iu.edu (JW), evesperi@indiana.edu (EV)

of initial conditions and IMFs and found that in no case complete energy equipartition was reached. The authors also find that the inner region of a cluster can get closer to energy equipartition than the outer region ($\eta_{max} \sim 0.15$), but after many relaxation times stars in different radial bins converge to a similar state of "partial equipartition" ($\eta \sim 0.08$). A similar conclusion was reached by Bianchini et al. (2016) using a set of Monte Carlo cluster simulations. While measurements of $\sigma(m)$ are becoming possible with Hubble Space Telescope proper motion studies and data from GAIA (e.g. Wright et al. 2016), measurements of the dependence of kinematical properties on mass are still challenging (e.g. Baldwin et al. 2016).

Since mass segregation is a direct consequence of a cluster's evolution towards energy equipartition, the degree of mass segregation within a cluster should be connected with the level of energy equipartition (Trenti & van der Marel 2013). Observational studies of globular clusters have recently been able to study how the radial distribution of stars depends on stellar mass by looking at how the slope of cluster's stellar mass function (α) changes with projected clustercentric distance (R) (Beccari et al. 2010; Frank et al. 2012, 2014; Dalessandro et al. 2015; Beccari et al. 2015; Zhang et al. 2015). With the exception of NGC 6101 (Dalessandro et al. 2015), the behaviour of $\alpha(R)$ in each cluster is such that the mass function is flatter (top-heavy) in the inner regions and steeper (bottom-heavy) in the outer regions of the cluster indicating the clusters are at least partially mass segregated.

In Webb & Vesperini (2016) we have quantified the radial variation in a cluster's mass function as δ_α, the slope of a plot of α versus $\ln(\frac{r}{r_m})$ where r and r_m are the clustercentric distance and half-mass radius respectively (presented in three-dimensions and in projection). We found that δ_α decreases from zero (no segregation) with time as a cluster segregates, with the rate at which δ_α decreases primarily depending on a cluster's initial half-mass relaxation time t_{rh} and tidal filling factor $\frac{r_m}{r_t}$ (where r_t is the cluster's tidal radius). We also find that δ_α reaches a similar minimum value for all our model clusters such that clusters never become fully mass segregated. We suggest that the existence of a minimum δ_α must be linked to the overwhelming evidence that clusters can only reach a minimum value of η that is greater than -0.5.

The purpose of this study is to use N-body simulations of star clusters with a range of initial conditions to study the co-evolution of a cluster's δ_α and η (both three dimensionally and in projection). Linking observational measurements of the degree of mass segregation in a cluster to its state of energy equipartition would provide a powerful tool for indirectly measuring energy equipartition in star clusters. In Section 2 we summarize the initial conditions of the N-body models initially studied in Webb & Vesperini (2016). In Section 3 we determine how δ_α and η evolve for model clusters with different sizes, binary fractions, IMFs, black hole retention fractions, and orbits in a Milky Way-like tidal field. To make our results useful for observations, we also determine whether or not projection effects can alter the apparent evolution of either δ_α or η. We discuss and summarize all of our findings in Section 4, where we introduce a method for inferring the value of η based simply on a measurement of δ_α.

2 N-BODY MODELS

As originally discussed in Webb & Vesperini (2016), the evolution of each model star cluster in our suite of simulations was simulated using the direct N-body code NBODY6 (Aarseth 2003). The initial positions and velocities of individual stars are generated assuming the cluster follows a Plummer density profile (Plummer 1911; Aarseth et al. 1974). The Plummer profile is cut-off at a radius of 10 times the cluster's initial half-mass radius $r_{m,i}$, with model clusters having $r_{m,i}$ equalling either 1.1 pc or 6 pc. The IMF used to generate the initial distribution of stellar masses has the functional form:

$$\frac{dN}{dm} = m^\alpha \tag{1}$$

where m represents stellar mass. For our main model clusters, the IMF is taken from Kroupa, Tout, & Gilmore (1993) (K93) where α equals -2.7 for $m > 1M_\odot$, -2.2 for $0.5 \leqslant m \leqslant 1M_\odot$, and -1.3 for $0.08 < m \leqslant 0.5M_\odot$. We restrict stellar masses to be between 0.1 and 50 $M_\odot$. The stellar evolution algorithm for individual stars is taken from Hurley et al. (2000) assuming all stars have the same metallicity (0.001).

Using a K93 IMF, our base models taken from Webb & Vesperini (2016) are $6 \times 10^4 M_\odot$ clusters with $r_{m,i}$ equalling 1.1 pc and 6 pc and circular orbits at 6 kpc in a Milky Way-like potential (RM1 and RM6 respectively). The Galactic potential consists of a $1.5 \times 10^{10} M_\odot$ point-mass bulge, a $5 \times 10^{10} M_\odot$ Miyamoto & Nagai (1975) disk (with $a = 4.5$ kpc and $b = 0.5$ kpc), and a logarithmic halo potential (Xue et al. 2008). The halo potential is scaled such that the circular velocity 8.5 kpc from the Galactic centre is 220 km/s. Since each cluster starts with the same tidal radius r_t, the 1.1 pc cluster is initially tidally under filling ($\frac{r_m}{r_t} = 0.04$) and the 6 pc cluster is initially tidally filling ($\frac{r_m}{r_t} = 0.2$).

To study the effects of different IMFs on the evolution of δ_α and η, model clusters with different IMFs from Webb & Vesperini (2016) with $r_{m,i} = 6$ pc and circular orbits at 6 kpc in the Milky Way-like potential (identical to RM6) are considered. In addition to the K93 IMF, we consider a Kroupa (2001) IMF (IMFK01), a Salpeter IMF with α =2.35 (Salpeter 1955) (IMF235), and a broken power law IMF with α equals -0.9 for $0.1 < m < 0.5M_\odot$ and -2.3 for $0.5 \leqslant m \leqslant 50M_\odot$ (IMFBPL). For non-K93 IMFs, the publicly available code McLuster (Küpper et al. 2011) is used to generate stellar masses.

To study a larger range of tidal filling factors, we make use of previous simulations from Leigh et al. (2013) and Webb & Leigh (2015) with circular orbits between 6 and 104 kpc, orbital eccentricities between 0 and 0.9, initial masses of $6 \times 10^4 M_\odot$, initial half mass radii of 1.1 pc and 6 pc, and primordial binary fractions of 4%. These models are named based on their eccentricity (E), circular orbit (R) or perigalactic (RP) distance, and initial $r_{m,i}$ (RM) such that, for example, a model cluster with an orbital eccentricity of 0.5, perigalactic distance of 6 kpc, and $r_{m,i} = 1.1$ pc is named E05RP6RM1. To generate binary star masses, the sum of two stars drawn from the IMF is set equal to the total binary mass and the mass ratio is randomly taken from a uniform distribution. The stellar evolution algorithm for binary stars is taken from Hurley et al. (2002), while the

initial distribution of orbital eccentricities and periods are taken from Heggie (1975) and Duquennoy & Mayor (1991) respectively. When analyzing the models all binaries are treated as unresolved.

In order to study the effects of black holes on the co-evolution of δ_α and η, we ensure that a set fraction of all newly formed black holes are not given a velocity kick. For the purposes of this study we consider black hole retention fractions of 25% (BH25) and 50% (BH50). Table 1 contains a summary of all the models discussed above.

3 THE EVOLUTION OF ENERGY EQUIPARTITION AND MASS SEGREGATION

As described in Webb & Vesperini (2016), to measure δ_α we first identify stars with masses within the desired mass range that the global mass mass function is going to be measured over. Commonly this mass range is either 0.1-0.5 $M_\odot$, 0.3-0.8 $M_\odot$, or 0.5-0.8 $M_\odot$ depending on the observational dataset. In this Section we will focus on the 0.1-0.5 $M_\odot$ mass range, however in Section 4 all three mass ranges will be discussed. To measure the slope of the global mass function, α_G, stars are first separated into 6 mass bins containing an equal number of stars. Keeping the bin width variable, such that each mass bin contains the same number of stars, allows for the cluster's mass function to determined with minimal numerical bias (Maíz Apellániz & Úbeda 2005). The value of m in each mass bin is set equal to the mean mass of stars within the mass bin. The slope of the line of best fit to $\frac{dN}{dm}$ versus m is then α_G.

To measure radial variation in the stellar mass function, we next separate the sub-population of stars within the given mass range into 10 radial bins. We again keep the width of each bin variable, such that each radial bin contains 10% of the total sub-population. The distance of each bin from the centre of the cluster is set equal to the mean r of all stars within the radial bin. After measuring α in each radial bin, δ_α is then equal to the slope of the line of best fit to α versus $\ln(\frac{r}{r_m})$. Repeating this process for each time step allows us to determine how δ_α evolves with time for each model cluster (see Webb & Vesperini (2016) for the evolution of δ_α with respect to time and α_G for each model cluster in Table 1).

To measure η we first identify stars with masses between 0.1 and 1.8 $M_\odot$ (similar to Bianchini et al. (2016)). Separating the sub-population into 10 mass bins containing an equal number of stars, we measure the velocity dispersion σ of all stars within the bin. Similar to our calculation of δ_α, the mean mass of all stars within the bin is used to set m. η is then equal to the slope of the line of best fit to $\log(\sigma)$ versus $\log(m)$.

Since η is expected to vary with distance from the cluster center (Trenti & van der Marel 2013; Bianchini et al. 2016), we have also explored the time evolution of η and δ_α including only stars within the half-mass radius. This constraint provides further insight into the evolution towards energy equipartition of the inner regions of a cluster. To compare with observational datasets, the calculations of both η and δ_α are repeated using each stars projected clustercentric radius (R) when radially binning the data and projected velocities to measure σ. And finally, to increase the number of stars used in each measurement of η and δ_α we group time steps in collections of three.

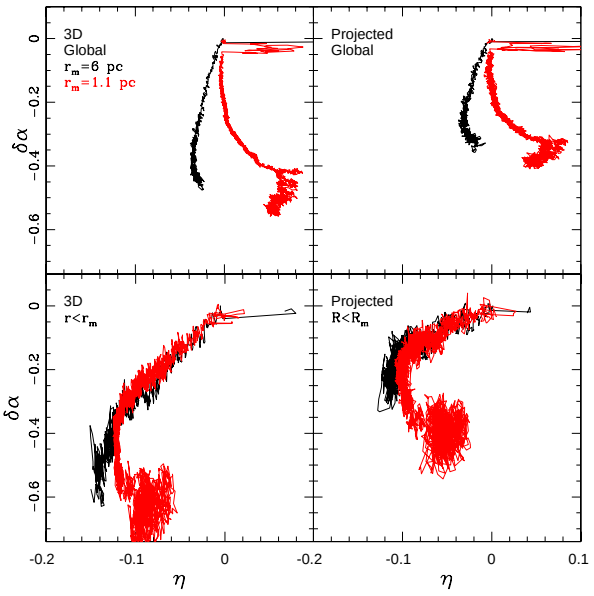

Figure 1. Evolution of η (for stars with $0.1 < m < 1.8$) as a function of δ_α (for stars with $0.1 < m < 0.5$) for stars in model clusters with circular orbits at 6 kpc in a Milky Way-like potential with $r_{m,i} = 1.1$ pc (red) and $r_{m,i} = 6$ pc (black). Upper Left Panel: η and δ_α are measured using the three dimensional position and velocity of all stars in the cluster. Lower Left Panel: η and δ_α are measured using the three dimensional position and velocity of stars with $r < r_m$. Upper Right Panel: η and δ_α are measured using the projected position and line of site velocity of all stars in the cluster. Lower Left Panel: η and δ_α are measured using the projected position and line of site velocity of stars with $R < R_m$.

3.1 Star Clusters with Different Tidal Filling Factors

We begin our study by presenting the evolution of η as a function of δ_α for the $6 \times 10^4 M_\odot$ model clusters with $r_{m,i} = 1.1$ pc and $r_{m,i} = 6$ pc, K93 IMFs, and circular orbits at 6 kpc in a Milky Way-like potential (Figure 1). As previously mentioned, the $r_{m,i} = 1.1$ pc is initially tidally under-filling while the $r_{m,i} = 6$ pc cluster is initially tidally filling. Each parameter is presented in three dimensions and in projection. Additionally, η and δ_α are calculated using both the entire stellar population and only for stars with $r < r_m$ (or $R <$ Projected half-mass radius (R_m) when considering clusters in projection) in order to compare inner and global cluster properties.

Considering first the three-dimensional evolution of η and δ_α using all stars in the cluster (Figure 1: Upper Left Panel), we see that η and δ_α initially decrease, as expected, for both the the $r_{m,i} = 1.1$ pc and $r_{m,i} = 6$ pc clusters. Early fluctuations in η are simply the result of remnants that have been given large velocity kicks which quickly escape the cluster. However it is not long before the evolution of both parameters in the two model clusters diverges, with η actually increasing while δ_α continues to decrease for the

Table 1. Model Input Parameters

Name	Mass	$r_{m,i}$	R_c	IMF
Star Clusters with Different Tidal Filling Factors [1]				
RM1	$6 \times 10^4 M_\odot$	1.1 pc	6 kpc	K93
RM6	$6 \times 10^4 M_\odot$	6 pc	6 kpc	K93
Clusters with Different IMFs[1]				
IMF235	$6 \times 10^4 M_\odot$	6 pc	6 kpc	$\alpha_0 = 2.35$
IMFK01	$6 \times 10^4 M_\odot$	6 pc	6 kpc	K01
IMFBPL	$6 \times 10^4 M_\odot$	6 pc	6 kpc	$\alpha_0 = -0.9$ for $0.1 < m < 0.5 M_\odot$ $\alpha_0 = -2.3$ for $0.5 \leqslant m \leqslant 50 M_\odot$.
Clusters with 4% Initial Binaries and Different Orbits [2]				
E0R6RM1	$6 \times 10^4 M_\odot$	1.1 pc	6 kpc	K93
E05RP6RM1	$6 \times 10^4 M_\odot$	1.1 pc	6 kpc	K93
E0R18RM1	$6 \times 10^4 M_\odot$	1.1 pc	18 kpc	K93
E05RP6RM6	$6 \times 10^4 M_\odot$	6 pc	6 kpc	K93
E0R18RM6	$6 \times 10^4 M_\odot$	6 pc	18 kpc	K93
E09RP6RM6	$6 \times 10^4 M_\odot$	6 pc	6 kpc	K93
E0R104RM6	$6 \times 10^4 M_\odot$	6 pc	104 kpc	K93
Star Clusters with Different Black Hole Retention Fractions[1]				
BH25	$6 \times 10^4 M_\odot$	6 pc	6 kpc	K93
BH50	$6 \times 10^4 M_\odot$	6 pc	6 kpc	K93

[1] Webb & Vesperini (2016)
[2] Webb et al. (2013), Leigh et al. (2013), Webb & Leigh (2015)

$r_{m,i} = 1.1$ pc cluster. Eventually, once η and δ_α decrease a little further, η starts increasing for the $r_{m,i} = 6$ pc cluster as well. Once the $r_{m,i} = 1.1$ pc cluster undergoes core collapse, the evolution of δ_α slows dramatically while η fluctuates about a mean value.

At first, an increase in η seems counterintuitive as clusters are supposed to be evolving towards a state of energy equipartition ($\eta \sim -0.5$). However, this discrepancy can be understood by remembering that 1) σ decreases with r, and 2) mean stellar mass starts to decrease with r as the cluster undergoes mass segregation. Hence, while energy equipartition can be on-going locally in a cluster, the combined effects of mass segregation and tidal stripping can cause the global value of η to increase with time. Since the under-filling cluster is able to expand more than the filling cluster, its velocity dispersion profile will be steeper and it will require less mass segregation (i.e a less negative δ_α) than the extended cluster before the global η starts to increase. Similar effects are seen when η and δ_α are measured in projection (Figure 1: Upper Right Panel), albeit to a lesser degree since line of site velocity dispersion does not depend as strongly on r.

To minimize the combined effects of local relaxation, mass segregation, and the radial dependence of σ on η, we instead focus on stars within a narrower radial range. In the lower panels of Figure 1 we consider the evolution of η and δ_α both in three dimensions (bottom left panel) and projection (bottom right panel) for stars with $r < r_m$ and $R < R_m$ respectively. In these lower panels we see that the co-evolution of η and δ_α is at first identical for the $r_{m,i} = 1.1$ pc and $r_{m,i} = 6$ pc clusters, with both parameters decreasing at similar linear rates. Both model clusters break from this linear relationship when $\delta_\alpha \sim -0.35$ and $\eta \sim -0.12$, as both parameters slow down due to cluster expansion with the local t_{rh} increasing throughout the cluster. Therefore the fact that clusters reach a minimum value of δ_α (as found by Webb & Vesperini (2016)) is directly linked to a clusters ability to only reach a state of partial energy equipartiion (Trenti & van der Marel 2013; Bianchini et al. 2016). For the more compact cluster with $r_{m,i} = 1.1$ pc, η eventually starts increasing while δ_α continues to decrease. Both parameters eventually reach final constant values in each model.

To understand why both model clusters break from the linear δ_α - η relationship, we consider the evolution of both parameters for all stars in the $r_{m,i} = 1.1$ pc model with $r < r_m$ with time in Figure 2. For comparison purposes we also consider the evolution of η within the 10%, 20%, 30% and 40% Lagrangian radii shells (as indicated in the legend) as well as the evolution of the 10% Lagrange radius itself. The top and bottom panels of Figure 2 illustrate that δ_α within r_m will decrease with time until the cluster approaches core collapse (at approximately 5.5 Gyr) and then remains more or less constant (in agreement with Giersz & Heggie (1996)). As the cluster continues to undergo repeated core collapse events ,δ_α will resume decreasing towards its final minimum value (albeit at a much slower rate) as the cluster decreases in size while it slowly dissolves. η within r_m on the other hand stops decreasing much sooner, around 2.5 Gyr, despite the fact that η is still decreasing locally within individual radial bins. This behaviour suggests that once a cluster reaches a high enough degree of mass segregation ($\delta_\alpha \sim -0.35$), the radial dependence of σ and mean stellar mass will even start to affect measurements of η over reduced radial ranges and η within r_m will stop de-

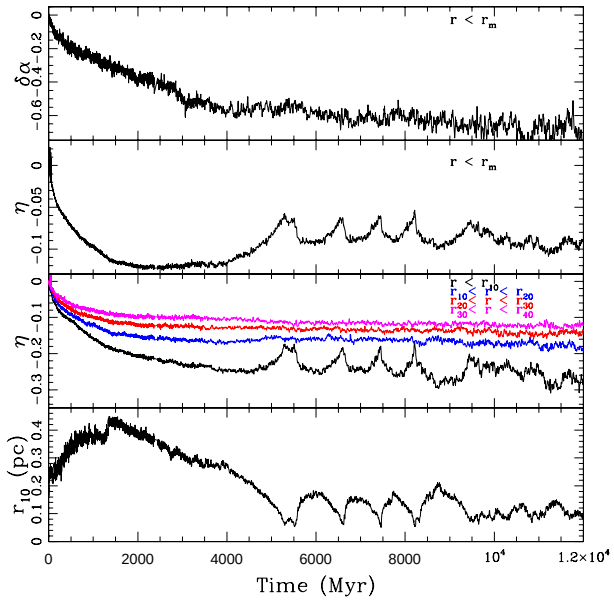

Figure 2. Evolution of δ_α for stars within r_m and $0.1 < m < 0.5$ (Top Panel), η for stars within r_m and $0.1 < m < 1.8$ (second panel from the top), η for stars within different Lagrange radii (second panel from the bottom) and the 10% Lagrange radius (Bottom Panel) as a function of time for a model cluster with $r_{m,i} = 1.1$ pc and a circular orbit at 6 kpc in a Milky Way-like potential.

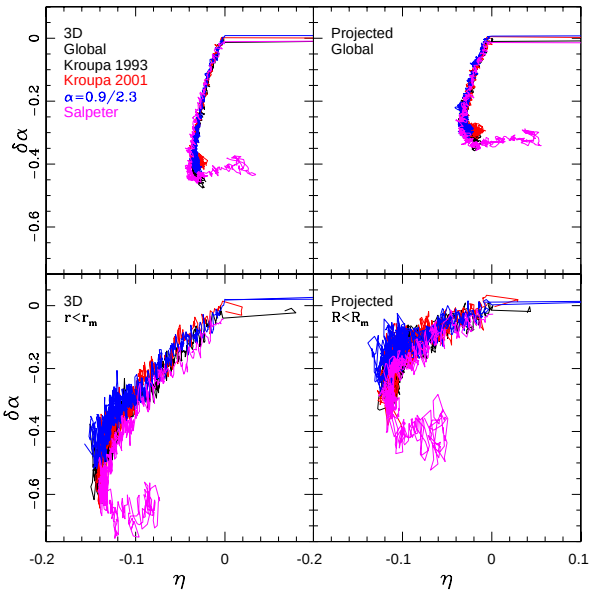

Figure 3. Evolution of η (for stars with $0.1 < m < 1.8$) as a function of δ_α (for stars with $0.1 < m < 0.5$) for stars in model clusters with circular orbits at 6 kpc in a Milky Way-like potential with a K93 IMF (black), K01 IMF (Red), broken power law IMF (blue) and Salpeter IMF (magenta). Upper Left Panel: η and δ_α are measured using the three dimensional position and velocity of all stars in the cluster. Lower Left Panel: η and δ_α are measured using the three dimensional position and velocity of stars with $r < r_m$. Upper Right Panel: η and δ_α are measured using the projected position and line of site velocity of all stars in the cluster. Lower Left Panel: η and δ_α are measured using the projected position and line of site velocity of stars with $R < R_m$.

creasing and start increasing in the same way the global η does. Therefore it is the combined effects of energy equipartition, mass segregation, and the radial dependence of σ that cause the relationship between δ_α and η for stars within r_m to break from linearity at later times. Below $\delta_\alpha \sim -0.35$, η does not stop decreasing as quickly in the $r_{m,i} = 6$ pc model because the radial dependence of σ is not as steep as the $r_{m,i} = 1.1$ pc model.

The increase in η for stars with $r < r_m$ becomes more rapid as the cluster approaches core collapse. The increase in η for all stars with $r < r_m$ is directly dependent on the behaviour of η in the core of the cluster, as massive stars preferentially interact with newly formed binary stars and their velocity dispersion increases. Hence, as the cluster approaches core collapse η is actually increasing locally within the core, and is not just a result of mass segregation and the dependence of σ on r. After the initial core collapse, η will fluctuate around a mean value as the cluster undergoes subsequent core collapse events, indicating that the mass segregation / energy equipartition process halts or has significantly slowed down in agreement with what is found in Giersz & Heggie (1996) & Heggie (1996).

3.2 Star Clusters with Different IMFs

To explore the effects of having a different IMF on the co-evolution of δ_α and η, we make use of simulations with $r_{m,i} = 6$ pc as in the tidally filling clusters above but with four different IMFs from Webb & Vesperini (2016). We consider a K01 IMF, Salpeter IMF, and a broken power-law IMF with α equals -0.9 for $0.1 < m < 0.5 M_\odot$ and -2.3 for $0.5 \leqslant m \leqslant 50 M_\odot$. From Figure 3 we see that the co-evolution of δ_α and η is IMF-independent, as all four models have very similar evolutionary tracks in three dimensions and in projection. Therefore the relationship between δ_α and η, including the linear relationship observed for stars with $r < r_m$ and $R < R_m$, is unaffected by whether or not the IMF is universal. A cluster's IMF, however, can influence where it is located on the δ_α - η evolutionary track at a given time if the cluster's structural evolution is also strongly affected. For example, the model with a Salpeter IMF will have a lower initial mass and expand less due to stellar evolution than the other clusters. These factors result in the Salpter IMF cluster having a shorter relaxation and reaching both the end of the linear evolutionary track (at $\delta_\alpha \sim -0.35$) and core collapse (causing η to increase) within 12 Gyr.

3.3 Star Clusters with Primordial Binaries, Different Orbits, and Different Black Hole Retention Fractions

Finally, to study the evolution of δ_α and η over the widest possible range of initial conditions, we consider model clusters with different orbits, binary fractions, and black hole retention fractions taken from Leigh et al. (2013), Webb & Leigh (2015), and Webb & Vesperini (2016). Including model clusters with $r_{m,i} = 1.1$ pc and $r_{m,i} = 6$ pc and different orbital distances (6 kpc, 18 kpc, 104 kpc)

allows for a large range of tidal filling factors to be explored. Including model clusters with $r_{m,i} = 1.1$ pc and $r_{m,i} = 6$ pc and having eccentric orbits (e=0.5 and 0.9) allows us to determine whether tidal heating and tidal shocks at perigalacticon (kept fixed at 6 kpc) affects the co-evolution of δ_α and η.

We find that the presence of primordial binaries does not affect the evolution of either η or δ_α, as model clusters in Figure 4 with $r_{m,i} = 1.1$ pc and $r_{m,i} = 6$ pc and circular orbits at 6 kpc are identical to those in Figure 1. Conversely, the upper panels of Figure 4 confirm our statements in Section 3.1 that the co-evolution of δ_α and η is significantly affected by a cluster's initial relaxation time, tidal filling factor, tidal heating and tidal shocks. The dependence on initial relaxation time is related to how quickly a cluster undergoes core collapse, as mass segregation and energy transfer slow down and eventually stop during the post-core collapse phase. The dependence on the tidal filling factor can be seen by comparing clusters with similar initial relaxation times (i.e. initial sizes) in Figure 4. Since under-filling clusters expand more from their initial state than filling clusters, they will develop a steeper σ profile and require less segregation before the global η starts increasing.

Model clusters with eccentric orbits are subject to tidal heating as they approach perigalacticon and a tidal shock at perigalactic, providing additional energy to stars orbiting in the outer regions of the cluster. Initially, before much segregation has taken place, tidal heating and shocks do not affect η or δ_α as the additional energy is dispersed among stars over the entire mass spectrum. However as δ_α continues to decrease, the additional energy starts to primarily go to the low mass stars which come to dominate the outer region of the cluster. The energy injection leads to increasing the velocity dispersion of low mass stars, which in turn causes η to briefly decrease when the cluster is near perigalacticon. However once these stars escape the cluster η returns to its normal evolution.

The strength of the external tidal field has a much lesser effect on stars in the core, such that η in the inner regions of filling and under-filling clusters will evolve self similarly. This point is illustrated in the lower panels of Figure 4 where the evolutionary tracks of all model clusters are nearly identical when only stars with either $r < r_m$ and $R < R_m$ are considered. For model clusters with identical initial relaxation times, the cluster's tidal filling factor is able to influence its location on the δ_α - η evolutionary track as under-filling clusters are able to expand more than filling clusters such that their relaxation time become longer. Hence $r_{m,i} = 6$ pc models e0r18, e09rp6, and e0r104 are just reaching the end of the linear portion of the δ_α - η evolutionary track after 12 Gyr while e0r6 and e05rp6 have evolved past it with δ_α values less than -0.35.

To illustrate the effects of retaining black holes, we have also plotted in Figure 4 model clusters from Webb & Vesperini (2016) with 25% and 50% black hole retention fractions at evenly spaced time steps (cyan and yellow respectively) up until they have lost the same amount of mass as model e0r6. As discussed in Webb & Vesperini (2016), the retention of black holes slows the mass segregation processes such that δ_α stops evolving at a higher (less negative) value in BH25 and BH50 than in e0r6 (also in agreement with Trenti et al. (2010); Lutzgendorf et al. (2013)). Figure 4 illustrates that η also behaves in a similar fashion. Hence the co-evolution of δ_α and η is unaffected by the presence of black holes in a star cluster up until the cluster approaches dissolution.

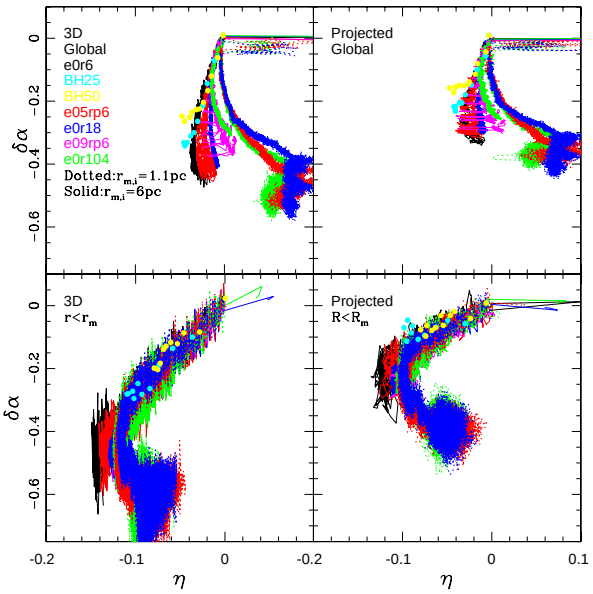

Figure 4. Evolution of η (for stars with $0.1 < m < 1.8$) as a function of δ_α (for stars with $0.1 < m < 0.5$) for stars in model clusters with circular orbits between 6 and 18 kpc, orbital eccentricities between 0 and 0.9, initial masses of $6 \times 10^4 M_\odot$, and initial half mass radii of 1.1 pc (dotted lines) and 6 pc (solid lines). Different model clusters are colour coded based on orbit, as indicated by the legend. Cyan and yellow data points correspond to model clusters with a circular orbit at 6 kpc and an initial half mass radius of 6 pc but with black hole retention fractions of 25% and 50% respectively. Upper Left Panel: η and δ_α are measured using the three dimensional position and velocity of all stars in the cluster. Lower Left Panel: η and δ_α are measured using the three dimensional position and velocity of stars with $r < r_m$. Upper Right Panel: η and δ_α are measured using the projected position and line of site velocity of all stars in the cluster. Lower Left Panel: η and δ_α are measured using the projected position and line of site velocity of stars with $R < R_m$.

4 DISCUSSION AND SUMMARY

Using a suite of N-body simulations, we have found that the co-evolution of a cluster's global η and global δ_α can be strongly affected its initial relaxation time and tidal filling factor. δ_α has previously been shown to decrease faster for clusters with shorter relaxation times, with a strong external tidal field having the capability of slowing δ_α's rate of decrease by stripping preferentially low mass stars from the cluster once some segregation has occurred (Webb & Vesperini 2016). And while the global η does initially decrease as expected, the combined effects of local relaxation, mass segregation, and the radial dependence of σ due to tidal stripping can all cause the global η to actually start increasing. This apparent increase makes the global η

a poor indicator of the degree of energy equipartition in a cluster.

The relationship between η and δ_α for stars with $r < r_m$ and $R < R_m$ on the other hand is linear and appears to be the same for all clusters independent of their initial conditions. The behaviour of both parameters is less affected by the strength of an external tidal field. Only strongly segregated clusters, characterized by a steep radial dependence in σ and mean stellar mass, and clusters that are undergoing or have undergone core collapse (such that mass segregation / energy equipartition has ended) will evolve away from this relation.

To quantify the linear portion of the relationship between η and δ_α for stars within r_m, we plot in Figure 5 the η and δ_α (measured using stars with $r < r_m$ (left panel) and $R < R_m$ (right panel)) for each model cluster in this study. We then fit a line of best fit to the data points which fall along the linear portion of each plot (highlighted in red) and measure its slope and y-intercept. As previously discussed, the linear portion of the track ends when δ_α (when measured using stars between 0.1 and 0.5 $M_\odot$) reaches -0.35 (-0.2 in projection), which causes η within r_m to stop decreasing due to the dependence of both mean stellar mass and σ on clustercentric distance. In order for our results to be applicable to a wide range of observational studies, the process is repeated for values of δ_α measured using stars with $0.3 < m < 0.8M_\odot$ (middle row) and $0.5 < m < 0.8M_\odot$ (lower row). Over these mass ranges, δ_α reaches -0.8 and -1.2 (-0.4 and -0.7 in projection) respectively by the time η stops decreasing. We report in Table 2 the slope and intercept (along with the error on the values of these parameters) of the best-fit line found via linear regression of each of the panels shown in Figure 5, as well as the coefficient of determination R^2 for each fit and the minimum value of δ_α for which the fits are applicable.

Figure 5 and Table 2 provide a direct link between energy equipartition and mass segregation (measured via radial variation in the stellar mass function) in star clusters. They also prove that the minimum value of δ_α reached by the models of Webb & Vesperini (2016) is the result of clusters only reaching a state of partial energy equipartition ($\eta < -0.5$) (Trenti & van der Marel 2013; Bianchini et al. 2016). The linear relationship between η and δ_α within r_m offers the possibility of inferring the kinematic properties of a star cluster from its photometric properties (and viceversa). The distribution of stellar masses in a cluster can be used to provide an indication of η without the need for spectroscopy or proper motions. Furthermore, if stellar masses and velocities are available within the same globular cluster, then clusters which do not fall on the linear relationship could potentially be identified as core-collapse clusters.

One factor that has not been explored by our suite of simulations is the effect of primordial mass segregation on the coevolution of η and δ_α. The effects of primordial mass segregation on δ_α were considered in Webb & Vesperini (2016), where it was determined that while primordial mass segregation alters the initial value of δ_α at time zero, a primordially mass segregated cluster will reach a similar δ_α than a non-primordially segregated cluster within a few relaxation times. What needs to be considered for the purposes of this study however is whether or not primordial mass segregation is linked to mass-dependent kinematical properties.

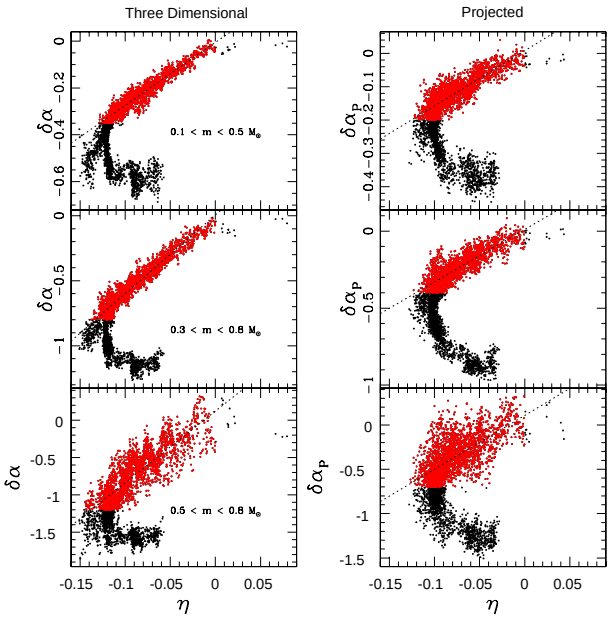

Figure 5. Evolution of η (for stars with $0.1 < m < 1.8$) as a function of δ_α (measured over different mass ranges) for stars within r_m of model clusters with circular orbits between 6 and 104 kpc, orbital eccentricities between 0 and 0.9, initial masses of $6 \times 10^4 M_\odot$, and initial half mass radii of 1.1 pc and 6 pc. In the left column the three dimensional positions and velocities are used to measure η and δ_α while in the right column the projected values of these quantities are used. In the top row only stars with $0.1 < m < 0.5M_\odot$ are used to calculate δ_α while in the middle and bottom columns stars $0.3 < m < 0.8M_\odot$ and $0.5 < m < 0.8M_\odot$ are used respectively. Red points show the values used for the calculation of the linear best-fit line shown as a dotted line in each panel. The numerical values of the parameters of each best-fit line are reported in Table 2.

Primordial mass segregation might be in part driven by early dynamics, it could be mainly due to the star formation process or a combination of star formation and early dynamics (Bonnell et al. 2001; McMillan et al. 2007; Moeckel & Bate 2010; Maschberger et al. 2010); in any case the relation between spatial segregation and the kinematical properties is in general non-trivial and its investigation is well beyond the scope of this study.

Our work provides a theoretical prediction for the relationship between η and δ_α, and can be used today to estimate η for clusters that have an accurately measured δ_α via wide field studies. With upcoming proper motion measurements from the Hubble Space Telescope and GAIA, it is becoming possible to actually measure η. Hence the predicted relationship between η and δ_α will soon be able to be observationally tested. Observational verification would serve as a clear indication that the initial conditions and long-term evolution of star clusters are well understood and strengthen the applicability of the η / δ_α relation as a tool for studying globular clusters. A disagreement between theory and observations on the other hand would indicate additional studies are necessary to determine what types of initial conditions (including primordial mass segregation) or dynamical processes could alter the co-evolution of η and δ_α found here.

Table 2. Lines of Best Fit

Mass Range	Slope	y-intercept	R^2	$\delta_{\alpha,min}$
$0.1 < m < 0.5M_\odot$				
3D	2.69 ± 0.02	0.005 ± 0.002	0.92	-0.35
2D	1.65 ± 0.02	0.008 ± 0.002	0.73	-0.2
$0.3 < m < 0.8M_\odot$				
3D	6.05 ± 0.03	0.005 ± 0.003	0.92	-0.8
2D	3.41 ± 0.05	0.011 ± 0.004	0.72	-0.4
$0.5 < m < 0.8M_\odot$				
3D	9.6 ± 0.1	0.12 ± 0.01	0.74	-1.2
2D	6.1 ± 0.1	0.11 ± 0.01	0.46	-0.7

ACKNOWLEDGEMENTS

This work was made possible in part by the facilities of the Shared Hierarchical Academic Research Computing Network (SHARCNET:www.sharcnet.ca) and Compute/Calcul Canada, in part by Lilly Endowment, Inc., through its support for the Indiana University Pervasive Technology Institute, and in part by the Indiana METACyt Initiative. The Indiana METACyt Initiative at IU is also supported in part by Lilly Endowment, Inc.

REFERENCES

Aarseth, S.J. 2003, Gravitational N-body Simulations: Tools and Algorithms (Cambridge Monographs on Mathematical Physics). Cambridge University Press, Cambridge
Aarseth, S., Hénon, M., Wielen, R., 1974, A&A, 37, 183
Baldwin, A.T., Watkins, L.L., van der Marel, R.P., Bianchini, P., Bellini, A., Anderson, J. 2016, ApJ, 827, 12
Baumgardt H., Makino J. 2003, MNRAS, 340, 227
Beccari, G., Pasquato, M., De Marchi, G., Dalessandro, E., Trenti, M., Gill, M. 2010, ApJ, 713, 194
Beccari, G., Dalessandro, E., Lanzoni, B., Ferraro, F.R., Bellazzini, M., Sollima, A. 2015, ApJ, 814, 144
Bianchini, P., van de Ven, G., Norris, M.A., Schinnerer, E. Varri, A.L. 2016, MNRAS, 458, 3644
Bonnell, I. A., Clarke, C. J., Bate, M. R., Pringle, J. E. 2001, MNRAS, 324, 573
Dalessandro, E., Ferraro, F. R., Massari, D., Lanzoni, B., Miocchi, P., Beccari, G. 2015, ApJ, 810, 40
Duquennoy, A. & Mayor, M. 1991, A&A, 248, 485
Frank, M.J., Hilker, M., Baumgardt, H., Ct, P., Grebel, E.K., Haghi, H., Kpper, A.H.W., Djorgovski, S. G. 2012, MNRAS, 423, 291
Frank, M.J., Grebel, E.K., Kpper, A.H. W. 2014, MNRAS, 443, 815
Fregeau, J. M. Joshi, K. J., Portegies Zwart, S. F., & Rasio, F. A. 2002, ApJ, 570, 171
Giersz M., Heggie D. C. 1996, MNRAS, 279, 1037
Heggie, D.C. 1975, MNRAS, 173, 729
Hurley, J. R., Pols, O.R., Tout, C.A. 2000, MNRAS, 315, 543
Hurley, J. R., Tout, C.A., Pols, O.R. 2002, MNRAS, 329, 897
Inagaki S. & Wiyanto P., 1984, PASJ, 36, 391
Inagaki S. & Saslaw W. C., 1985, ApJ, 292, 339
Khalisi, E., Amaro-Seoane, P. and Spurzem, R. 2007, MNRAS, 374, 703
Kroupa, P., Tout C.A., Gilmore, G. 1993, MNRAS, 262, 545
Kroupa P. 2001, MNRAS, 322, 231
Küpper A. H. W., Maschberger, T., Kroupa, P., Baumgardt, H. 2011, MNRAS ,417, 2300
Leigh, N., Giersz, M., Webb, J.J., Hypki, A., de Marchi, G., Kroupa, P., Sills, A. 2013, MNRAS, 436, 3399
Lightman A. P. & Fall S. M., 1978, ApJ, 221, 567
Lutzgendorf, N., Baumgardt, H., Kruijssen, J.M.D. 2013, A&A, 558, A117
Maíz Apellániz, J., Úbeda, L. 2005, ApJ, 629, 873
Maschberger Th, Clarke, C.J., Bonnell, I. A., Kroupa, P. 2010 MNRAS, 404, 1061
McMillan S.L.W., Vesperini E., Portegies Zwart S. 2007, ApJ, 655, L45
Miyamoto, M. & Nagai, R. 1975, PASJ, 27, 533
Moeckel N. & Bate M.R. 2010, MNRAS 404, 721
Parker, R.J., Goodwin, S.P., Wright, N.J., Meyer, M.R., Quanz, S.P. 2016, MNRAS Letters, Accepted, arXiv:1604.00394
Plummer, H.C. 1911, MNRAS, 71, 460
Salpeter, E.E. 1955, ApJ, 121, 161
Spera, M., Mapelli, M., Jeffries, R.D. 2016, MNRAS, 460, 317
Spitzer L. Jr. 1969, ApJL, 158, 139
Spitzer, L.J. & Hart, M.H. 1971, ApJ, 164, 399
Spitzer L. Jr. 1987, Dynamical Evolution of GCs (Princeton, NJ: Princeton Univ. Press)
Trenti, M., Vesperini, E., Pasquato, M. 2010, ApJ, 708, 1598
Trenti M., van der Marel, R. 2013, MNRAS, 435, 3272
Vishniac, E. T. 1978, ApJ, 223, 986
Watters, W. A., Joshi, K. J., Rasio, F. A. 2000, ApJ, 539, 331
Webb, J.J., Harris, W.E., Sills, A., Hurley, J.R. 2013, ApJ, 764, 124
Webb, J.J. & Leigh, N. 2015, MNRAS, 453, 3278
Webb, J.J. & Vesperini, E. 2016, MNRAS, Accepted, arXiv:1608.07293
Wright, N.J., Bouy, H., Drew, J.E., Sarro, L.M., Bertin, E., Cuillandre, J, Barrado, D. 2016, MNRAS, 460, 2593
Xue, X.X. et al., 2008, ApJ, 684, 1143
Zhang, C. et al. 2015, ApJ, 815, 95

This paper has been typeset from a TEX/ LATEX file prepared
by the author.